Sains Malaysiana 39(2)(2010): 267–273

Preparation and Characterization of Calcium Phosphate Nanorods using Reverse Microemulsion and Hydrothermal Processing Routes

(Penyediaan dan Pencirian Nanorod Kalsium Fosfat melalui Kaedah Microemulsi Songsang dan Hidroterma)

H.N. LIM*, A. KASSIM & N.M. HUANG

ABSTRACT

Brushite (BR) and hydroxyapatite (HA) nanoparticles were fabricated through reverse microemulsion and hydrothermal processing route, respectively. The processing routes influenced nucleation and crystal growth although both methods resulted in nanorods formation. The calcium-to-phosphate ratio was 1.67, similar to that of natural bone and teeth. X-ray diffraction patterns revealed that the nanorods possessed almost pure crystal phase with negligible second phase. The ratio of particle length-to-width of BR and HA were approximately 3 and 4, respectively. To mimic the natural bone, chitosan/brushite (CTS/BR) and chitosan/hydroxyapatite (CTS/HA) nanocomposite scaffolds were prepared through rapid freeze-drying technique. The compressive strength of CTS/BR and CTS/HA nanocomposite scaffolds was compared for the first time. The compression test revealed that both the nanocomposite scaffolds exhibited reasonably high compressive strength of approximately 7 MPa. This value falls in the high-end range of cancellous bone's compressive strength, with the compressive strength of CTS/HA 0.88 MPa more than CTS/BR.

Keywords: Calcium phosphate nanoparticles; compressive strength; crystal growth; hydrothermal; microemulsion

ABSTRAK

Nanozarah brushit (BR) dan nanozarah hidroksiapatoit (HA) masing-masing disediakan melalui kaedah mikroemulsi songsang dan hidroterma. Kedua-dua kaedah penyediaan nanozarah mempengaruhi penukleusan dan pertumbuhan hablur walaupun kaedah-kaedah tersebut menghasilkan nanorod. Nisbah kalsium kepada fosfat ialah 1.67, serupa dengan nisbah tulang dan gigi asli. Corak pembelauan sinar-X menunjukkan kedua-dua nanorod itu memiliki fasa hablur yang hampir tulen dengan kehadiran fasa kedua yang boleh diabaikan. Nisbah panjang kepada lebar zarah bagi BR dan HA adalah masing-masing lebih kurang 3 dan 4. Untuk meniru tulang asli, rangka nanokomposit kitosan/brushit (CTS/BR) dan kitosan/hidroksiapatit (CTS/HA) disediakan menerusi teknik sejuk beku pantas. Kekuatan mampatan rangka nanokomposit CTS/BR dan CTS/HA telah dibandingkan buat pertama kali. Ujian mampatan menunjukkan kekuatan mampatan yang memuaskan bagi kedua-dua rangka nanokomposit, iaitu lebih kurang 7 MPa. Nilai ini berada dalam julat kekuatan di sebelah hujung tinggi bagi tulang kancelus, dengan kekuatan mampatan CTS/HA 0.88 MPa melebihi CTS/BR.

Kata kunci: hidroterma; kekuatan mampatan; mikroemulsi; nanozarah kalsium fosfat; pertumbuhan hablur

INTRODUCTION

Calcium phosphates which constitute the major inorganic phase of human hard tissues like the bone and teeth, are bioactive and can be rapidly integrated into the human body (Hench 1991; Weiner & Wagner 1998). The natural bone is made of calcium phosphate nanoparticles scattered in the organic matrix (Vallet-Regi & Gonzalez-Calbet 2004). Calcium phosphate has the general formula $Ca_{10-x}(HPO_4)_x(PO_4)_{6-x}(OH)_{2-x}$, with $0 \leq x < 2$. In this family, two compounds that attract attention are brushite (BR) and hydroxyapatite (HA). BR and HA are the subjects of intensive investigations as implant materials and coatings (Gbureck 2005; Hench 1993; Jarcho 1981; Legeros 1998). Both compounds are considered biocompatible and bioactive in the sense of osteoconduction and resorbability. BR is resorbed faster as it is a thermodynamically metastable compound under physiological conditions (Theiss et al. 2005). HA degrades considerably slower (Nilsson et al. 2002) given that it is nearly insoluble at normal physiological pH (Baksh 2000).

Reverse microemulsion processing route can be used to synthesize calcium phosphates in the range of nanometers besides having a minimised degree of agglomeration and controlled morphology of nanoparticles. The water-in-oil microemulsion is a transparent, isotropic liquid media with nanosized water droplets that are dispersed in a continuous oil phase and stabilized by surfactant molecules at the water/oil interface. The surfactant stabilised discontinuous water phase acts like a nanoreactor that can control nucleation and growth of fine and monodispersed particles in restricted geometries (Fendler 1987; Paul & Moulik 1997).

The hydrothermal technique produces calcium phosphate nanoparticles with a high degree of crystallinity and a calcium-to-phosphate ratio close to the stoichiometric value (Byrappa 2001). Wang et al. (2006) reported that nucleation and crystal growth processes mediated by macromolecule control would result in uniform products. The molecule-template addition has exerted significant control on the crystal morphology. Organized organic surfaces can control the nucleation of inorganic materials by geometric, electrostatic and stereochemical complementarities between the incipient nuclei and the functionalized substrates.

In this paper, we utilized sucrose ester S1670 as nonionic food grade surfactant to form water-in-oil (w/o) reversed microemulsion (water/heptan-1-ol/sucrose ester) as a soft template for the synthesis of brushite (BR) nanorods. Hydroxyapatite (HA) nanorods were prepared through hydrothermal method using triethanolamine to regulate nucleation and crystal growth. The formation mechanisms of BR and HA nanorods were discussed. Calcium phosphates have relatively low strength and are susceptible to fracture due to their brittleness (Xu et al. 2005). The biocompatibility, biodegradability, and nontoxicity of chitosan resemble the properties of collagen matrix (Ding 2007). Hybrid nanocomposite scaffolds made up of chitosan and calcium phosphates mimic the morphology and properties of natural bone. It is hope that the scaffolds can overcome the problem of the brittleness in calcium phosphates, besides possessing good biocompatibility, high bioactivity and great bone-bonding properties. The mechanical strength of chitosan/brushite (CTS/BR) and chitosan/hydroxyapatite (CTS/HA) nanocomposite scaffolds were compared for the first time.

Experimental Materials

The materials used in this work were calcium chloride, $CaCl_2$ (Sigma-Aldrich), disodium hydrogen phosphate, Na_2HPO_4 (Sigma-Aldrich), triethanolamine (Merck), heptan-1-ol (Merck), food grade sucrose monostearate (Mitsubishi-Kagaku Foods Corporation), medium molecular weight chitosan (Merck), acetic acid (Merck) and glutaraldehyde 25% (Unilab). All reagents were of analytical grade and were used as received. Deionised water with eletrical resistivity of 18.2 MΩ cm was used throughout the study.

For fabrication of BR nanorods, sucrose ester was mixed thoroughly with heptan-1-ol with sucrose ester-to-heptan-1-ol weight ratio equivalent to 0.80. Next, 0.30 M $CaCl_2$ and 0.18 M Na_2HPO_4 aqueous solutions were added into the mixture one after another under constant stirring to form a transparent reverse microemulsion. The microemulsion was aged at 40°C for seven days. The hydrothermal process for the fabrication of HA nanorods was carried out by mixing 0.30 M $CaCl_2$ and 0.18 M Na_2HPO_4 aqueous solutions. Then, 50 wt% triethanolamine was dissolved completely into the mixture. The mixed solution was stirred for 2 h to ensure the completion of cooperative interaction and self-assembly process. The final milky suspension was put in a teflon vessel, sealed tightly and heated in an oven at 180°C for 24 h. The obtained precipitates from both methods were then filtered off and washed thoroughly with ethanol and deionised water to remove the residual organic matters and ions. The precipitates were calcined at 600°C for 24 h to yield white powders.

The CTS/BR and CTS/HA nanocomposite scaffolds were prepared by solid–liquid phase separation and subsequent sublimation of solvent which has been previously described (Zhao et al. 2002). The nanorods (1.0 wt%) were dispersed in 100 mL of deionised water. CTS (1.0 wt%) was introduced under agitation, followed by the addition of 1.0 vol% acetic acid. The mixture was stirred for 5 min after adding 30 vol% aqueous glutaraldehyde (GA) at a 30:1 volume ratio of CTS-to-GA. Sequentially, the mixture was cast into a glass mold of 12 mm diameter × 12 mm height. To avoid phase separation between the nanorods and CTS solution, the mixture was rapidly transferred into a refrigerator at 4°C for 0.5 h to undergo the cross-linking reaction. Then, it was rapidly transferred to a freezer at -40°C to solidify the mixture and induce solid–liquid phase separation. The solidified mixture was maintained at that temperature for 2 h and was transferred into a freeze-drying vessel. The sample was finally freeze-dried at -40°C for 48 h, resulting in cylinders (Figure 1), which were stored under vacuum. Scaffolds that did not contain any nanorods were used as control.

Crystallinity of the powders was measured using a Phillips X-Ray Diffractometry (XRD). Measurements were taken from $2\theta = 4$ to 70^o at a size step of 0.033^o/s. The Cu anode X-ray was operated at 40 kV and 30 mA in combination with a Ni filter to give monochromatic Cu K_α radiation at 1.54 Å. The pattern was processed using PANalytical X'pert HighScore diffraction software to monitor the peak position and its corresponding intensity data. Chemical bonding of the powders was analyzed using a PerkinElmer Fourier Transform Infrared (FTIR) spectroscopy. The powders were mixed with potassium bromate, ground homogenously and converted into pellets. The spectra (% transmittance with wavenumber) were recorded.

The size and morphology of the powders were observed using a Phillips HMG 400 Transmission Electron Microscopy (TEM) with a 100 kV accelerating voltage. The powders were dispersed in ethanol and sonicated for five minutes to free them from aggregations. The mixtures were then placed on carbon-coated 400 mesh copper grids and dried at room temperature overnight before examination. The morphology of the scaffolds was observed using a LEO 1455 Variable Pressure Scanning Electron Microscopy (VPSEM) equipped with an Energy Dispersive X-Ray Analyzer (EDX). The scaffolds were mounted on aluminium stubs using double-sided tape and vacuumed coated with gold in a Polaron SC500 sputter coater.

Three specimens for each scaffold were cylindrical in shape with 12 mm diameter × 12 mm height. An Instron mechanical tester with 1 kN load cell was used

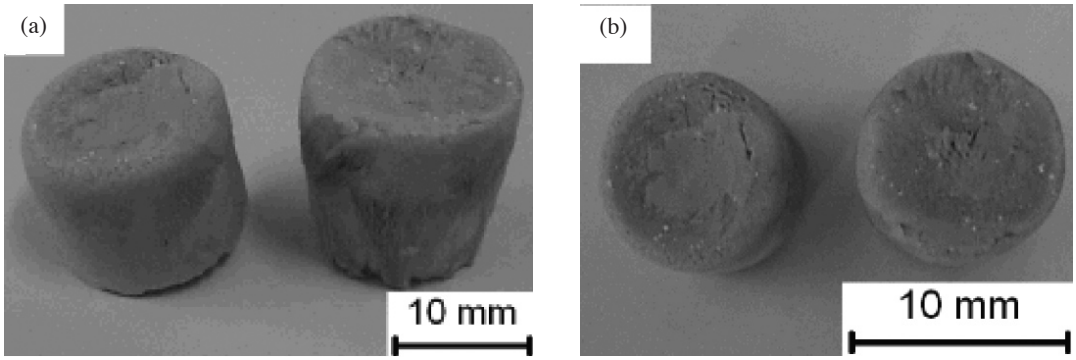

FIGURE 1. CTS/BR nanocomposite scaffolds (a) and view from the top (b)

for the compression test. The crosshead speed was set at 5 mm/s and the load was applied until the scaffolds were completely crushed. The compressive strength mean and standard deviation were calculated.

RESULTS AND DISCUSSION

Figure 2 shows the XRD patterns of the BR and HA nanorods indexed to brushite (JCPDS file no. 2-0085) and hydroxyapatite (JCPDS file no. 24-0033) crystal phases, respectively. Each sample contained negligible amount of second phase. The intensity of the diffraction peaks indicates that the nanorods are fairly well-crystallized. It was found that the intensity for BR is relatively higher at $2\theta = 29.5^{o}$ than the standard due to their preferential growth along a certain crystal plane resulted by their constraint in the micelles and influence of the micelle shape. The result is consistent with the TEM observation in Figure 4a which shows the morphology of rod-like nanoparticles. This phenomenon is not observed in HA due to its relatively smaller particle size, which resulted in weaker crystallinity.

Figure 3 shows the FTIR spectra of the and HA nanorods. The spectra exhibit easily distinguishable bands attributed to PO_4^{3-}. Generally, BR has more bands than HA due to its relatively larger particle size and better crystallinity. The bands at 560 cm^{-1} and 725 cm^{-1} were assigned to υ_4 O-P-O bending mode and phosphate group bending mode, respectively (Vallet-Regi & Gonzalez-Calbet 2004, Lu et al. 2006). The bands at 950 cm^{-1} and 990-1250 cm^{-1} were assigned to υ_1 symmetric P-O stretching mode and υ_3 antisymmetric P-O stretching mode, respectively (Wang et al. 2005). The PO_4^{3-} bands split at 1125 cm^{-1} for BR suggests high crystallinity which is consistent with the XRD result. The absence of split for HA is due to its comparatively smaller particle size, which affected its crystallinity.

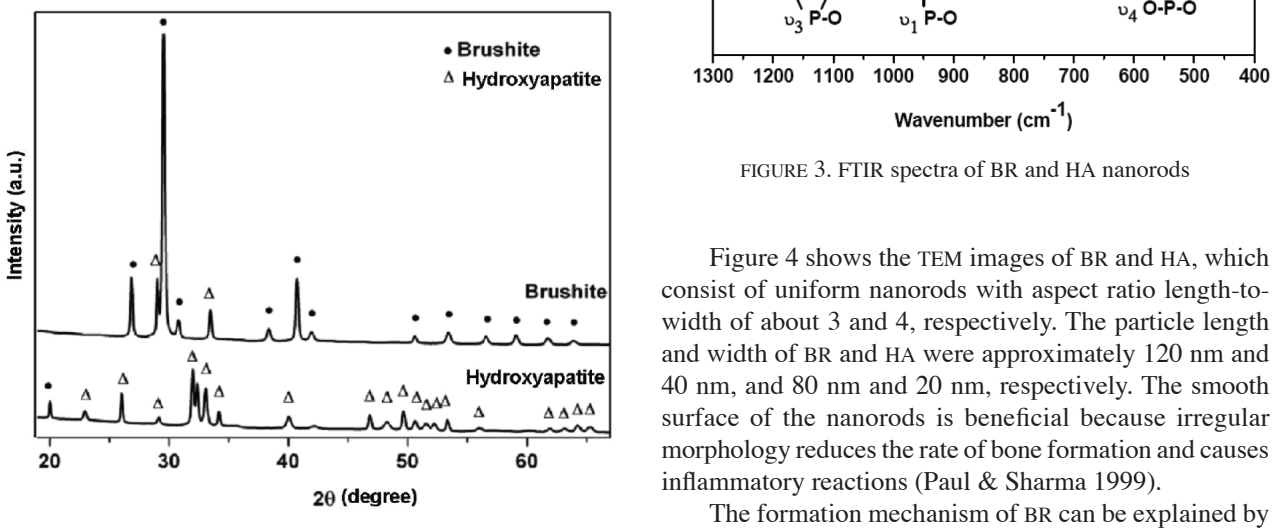

FIGURE 2. XRD analyses of BR and HA nanorods

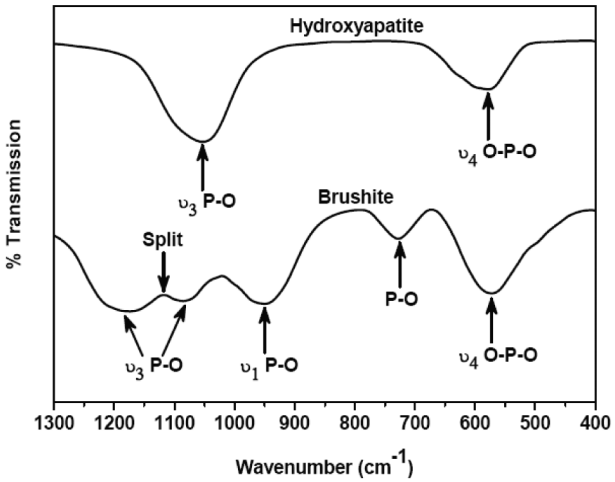

FIGURE 3. FTIR spectra of BR and HA nanorods

Figure 4 shows the TEM images of BR and HA, which consist of uniform nanorods with aspect ratio length-to-width of about 3 and 4, respectively. The particle length and width of BR and HA were approximately 120 nm and 40 nm, and 80 nm and 20 nm, respectively. The smooth surface of the nanorods is beneficial because irregular morphology reduces the rate of bone formation and causes inflammatory reactions (Paul & Sharma 1999).

The formation mechanism of BR can be explained by taking the sucrose ester micelles interaction into account.

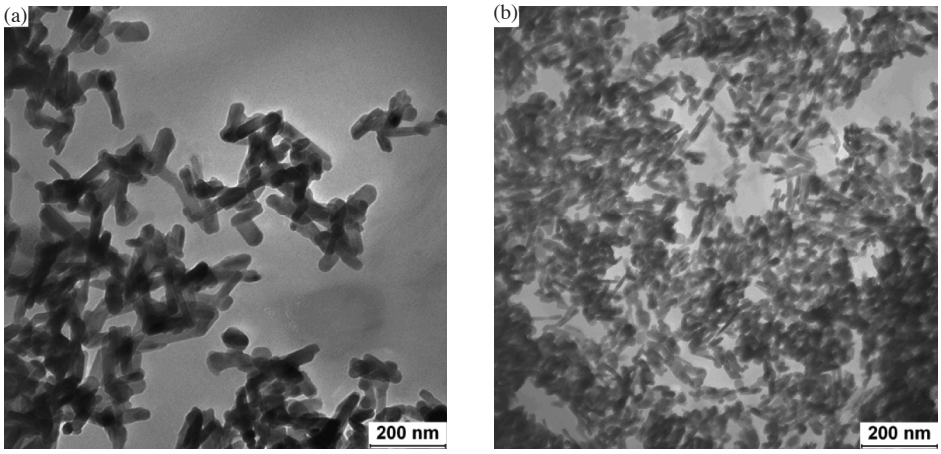

FIGURE 4. TEM images of BR (a) and HA (b) nanorods

Without water, the micelles are close to a compact globular structure but with the presence of water, the micelles become elongated or polydisperse because they strongly overlap (Glatter et al. 2001). Micelles containing calcium and phosphate ions collide due to Brownian motion, which result in fusion of the micelles and exchange of the contents within the cores (Pileni 2006). Therefore, nucleation and crystal growth happen in the newly formed micelles, leading to nanorods.

Triethanolamine (TEA) is a complexing agent which acts as a template in the hydrothermal process. The behaviour of TEA may correlate to a process called molecule recognition that could have taken place at the inorganic/organic interface due to charge and stereochemistry complementarity (Gray et al. 1997; Walsh et al. 1993). In an aqueous system, TEA would ionize completely and result in a tetrahedral structure with lone pair electrons. Thus, calcium cations can be incorporated to TEA by the charge (Figure 5). A plausible mechanism for the templating process is that TEA-Ca^{2+} complexes form rod-like micelles, which contain many calcium cations on the surface. With the presence of phosphate anions, the micelles act as nucleating points for the growth of HA crystals. During the hydrothermal stage, TEA-HA complexes are produced and they coalesce to control the morphology and size of obtained HA. Since the crystallization process is under critical control of TEA, the resulting HA nanoparticles were invariably nanorods with uniform morphology and controlled size (Wang et al. 2006).

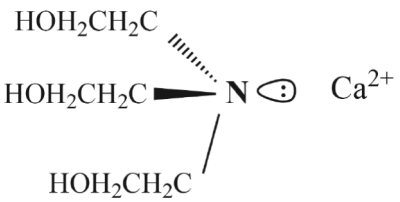

FIGURE 5. A schematic drawing of the complementarity between the lone pair electrons of TEA and calcium cation

Observation under SEM reveals porous structure of the scaffolds with pore width in a range of 10 – 100 μm (Figure 6). The presence of nanorods did not influence the formation of scaffolds as the morphology and pore size of the nanocomposite scaffolds, represented by CTS/BR (Figure 6b), were similar to that of the CTS scaffold (Figure 6a). The nanorods were well-distributed within the scaffold as shown by EDX (Figure 7). The composition of calcium, phosphate and oxygen elements of calcium phosphates were well-integrated with the carbon and oxygen elements of chitosan. This shows that only a small amount of CTS/GA in aqueous solution was sufficient to suspend the nanorods homogenously within the organic matrix.

The nanocomposite scaffolds mimic biologically produced inorganic-organic composites, like bone and teeth, in which self-assembled proteins and lipids form the structural scaffolding for the deposition of inorganic compounds (Lowenstam et al. 1989). They are hierarchically structured composites in which soft organic materials are organized on length scales of 1-100 μm used as frameworks for specifically oriented and shaped crystals (Levi-Kalisman et al. 2001). The internal architectural attributes, including pore size, shape and interconnectivity play an important role in the in vivo and mechanical performance of the implants. They control the degree of bone regeneration (Jin et al. 2000), path of bone regeneration (Le Huec et al. 1995) and determine the mechanical properties of the implants (Dean-Mo 1997). The ideal structures must be formed by an interconnected porous network with a wide variety of pore sizes. Large pores allow tissue ingrowth and vascularization of the newly formed tissue whereas pores in the microporous range promote protein adhesion and consequently cell adhesion and proliferation (Navarro et al. 2004). Optimum pore diameter depends on the size of the bone substitute - larger piece requires larger pores, keeping the total porosity constant (Bohner 2000).

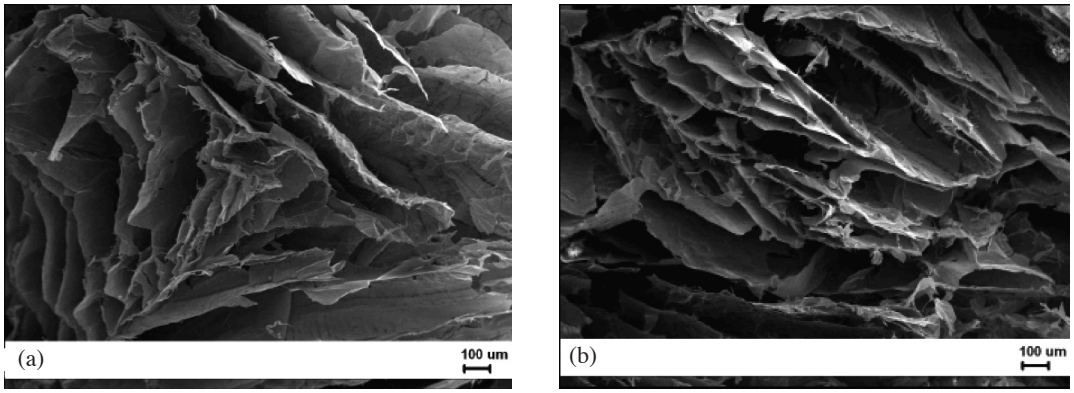

FIGURE 6. Morphology of CTS (a) and CTS/BR (b) scaffolds

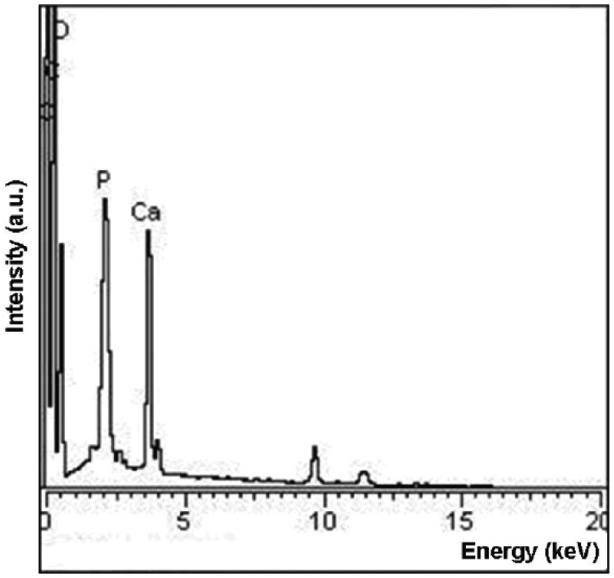

FIGURE 7. EDX of CTS/BR scaffold

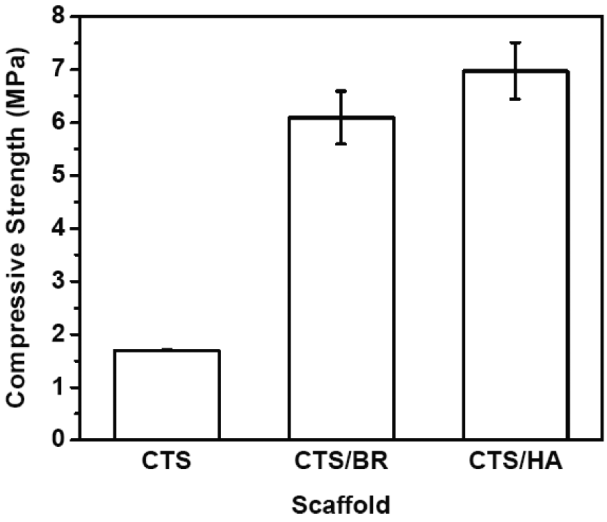

FIGURE 8. Compressive strength of scaffolds

Figure 8 shows the compressive strength of nanocomposite scaffolds. Each bar corresponds to the average numerical value of the three specimens for each sample. It is clearly shown that the compressive strength of the nanocomposite scaffolds were four-times higher than CTS's. The presence of the nanorods resulted in a fairly-high compressive strength. Both the nanocomposite scaffolds have desirable compressive strength of approximately 7 MPa, comparable to the high-end values of cancellous bone at 2-10 MPa (Ramay & Zhang 2004). The compressive strength of CTS/HA is slightly higher than CTS/BR by 0.88 MPa because with the same mass of nanorods, the higher number of narrower-sized HA particles leads to denser packing, which contributes to the higher compressive strength. Based on the previous studies (Knudsen 1959; Petch 1953; Rice 1993) the compressive strength of the ceramics increased as the grain size decreased. The nanocomposite scaffolds with fairly high compressive strength could act as reinforcing phase as well as bioactive phase for the smooth process of bone growth.

CONCLUSION

BR and HA nanorods were successfully fabricated using sucrose ester based reverse microemulsion and hydrothermal with TEA complexing agent as a template, respectively. The size of BR is visibly larger than HA due to the ease of overlapping among the sucrose ester micelles. The size and morphology of HA were well-controlled by TEA. Both the nanocomposite scaffolds had varying degree of pore size and appreciable compressive strength, which can be used as a precursor phase for bone implantation. The retention time for conducting bone tissue growth can be tailored by embedding calcium phosphate nanorods of different crystalline phases within the chitosan matrix. CTS/HA nanocomposite scaffold can well be used if slower resorption is preferred as HA degrades considerably slower at physiological conditions. On the other hand, CTS/BR nanocomposite scaffold will promote faster resorption at physiological conditions.

ACKNOWLEDGEMENT

H.N. Lim thank the Graduate Research Fellowship of Universiti Putra Malaysia for the financial support.

REFERENCES

Baksh, D. 2000. Design strategies for 3-dimensional in vitro bone growth in tissue-engineering scaffolds. In Davies, J. E. (ed.). *Bone engineering* p. 488-495. Toronto: Em Square.

Bohner, M. 2000. Calcium orthophosphates in medicine: from ceramics to calcium phosphate cements. *Injury* 31: 37-47.

Byrappa, K. 2001. *Handbook of Hydrothermal Technology.* LLC: Noyes Publications/ William Andrew Publishing.

Dean-Mo, L. 1997. Fabrication of hydroxyapatite ceramics with controlled porosity. *Journal of Materials Science: Materials in Medicine* 8: 227-232.

Ding, S.J. 2007. Biodegradation behavior of chitosan/calcium phosphate composites. *Journal of Non-Crystalline Solids* 353: 2367-2373.

Fendler, J.H. 1987. Atomic and molecular clusters in membrane mimetic chemistry. *Chemistry Review* 87: 877-899.

Gbureck, U., Dembski, S., Thull, R. & Barralet, J.E. 2005. Factors influencing calcium phosphate cement shelf-life. *Biomaterials* 26: 3691-3697.

Glatter, O., Orthaber, D. Stradner, A., Scherf, G., Fanun, M., Garti, N., Clement, V. & Leser, M.E. 2001. Sugar-ester nonionic microemulsion: structural characterization *Journal of Colloid Interface Science* 241: 215-225.

Gray, D.H., Hu, S., Juang, E. & Gin, D.L. 1997. Highly Ordered Polymer–Inorganic Nanocomposites via Monomer Self-Assembly: In Situ Condensation Approach. *Advance Materials* 9: 731-736.

Hench, L.L. 1991. Bioceramics: from concept to clinic. *Journal of American Ceramic Society* 74: 1487-1510.

Hench, L.L. 1993. Bioceramic: from concepts to clinics. *American Ceramic Society Bulletin* 72: 93-98.

Jarcho, M. 1981. Calcium phosphate ceramics as hard tissue prosthesis. *Clinical Orthopaedics and Related Research* 157: 259-278.

Jin, Q. M., Takita, H. & Kohgo, T. 2000. Effects of the geometry of hydroxyapatiteas cell substratum in BMP-induced ectopic bone formation. *Journal of Biomedical Materials Research* 51: 491-1.

Knudsen, F.P. 1959. Dependence of mechanical strength of brittle polycrystalline specimens on porosity and grain size. *Journal of American Ceramic Society* 42: 376-387.

Le Huec, J.C., Schaeverbeke, T., Clement, D. 1995. Influence of porosity on the mechanical resistance of hydroxyapatite ceramics under compressive stress. *Biomaterials* 16: 113-8.

Legeros, L.Z. 1998. Calcium phosphate materials in restorative dentistry: a review. *Advances in Dental Research* 2: 164-183.

Levi-Kalisman, Y., Addadi, L. & Weiner, S. 2001. Structure of the nacreous layer of a bivalve mollusk shell examined in the hydrated state using cryo-TEM. *Journal of Structural Biology* 135: 8-17.

Lowenstam, H.A., Weiner, S., Mann, S., Webb, J. & Williams, R. J. P. 1989. *On Biomineralization* New York: VCH Press.

Lu, X., Wang, Y., Wang, J., Qu, S., Weng, J., Xin, R. & Leng, Y. 2006. Calcium phosphate crystal growth under controlled environment through urea hydrolysis. *Journal Crystal Growth* 297: 396-402.

Navarro, M., del Velle, S., Martinez, S., Zeppetelli, S., Ambrosio, L., Planell, J.A. & Ginebra, M.P. 2004. New macroporous calcium phosphate glass ceramic for guided bone regeneration. *Biomaterials* 25: 4233-4241.

Nilsson, M., Fernandez, E., Sarda, S., Lidgren, L. & Planell, J. A. 2002. Characterization of a novel calcium phosphate/ sulphate bone cement. *Journal of Biomedical Materials Research* 61: 600-607.

Paul, B.K. & Moulik S. P. 1997. Microemulsions: an overview. *Journal of Dispersion Science and Technology* 18: 301-367.

Paul, W. & Sharma, C.P. 1999. Development of porous spherical hydroxyapatite granules: application towards protein delivery. *Journal of Materials Science* 10: 383-388.

Petch, N.J. 1953. The cleavage strength of polycrystals. *Journal of the Iron and Steel Institute* 174: 25-28.

Pileni, M.P. 2006. Reverse micelles used as templates: a new understanding in the nanocrystal growth of silver and copper nanocrystals by using hydrazine as redusing agent. *Journal of Experimental Nanoscience* 1: 13-27.

Ramay, H.R.R. & Zhang, M. 2004. Biphasic calcium phosphate nanocomposite porous scaffolds for load-bearing bone tissue engineering. *Biomaterials* 25: 5171-5180.

Rice, R.W. 1993. Comparison of stress concentration versus minimum solid area based mechanical property—porosity relations. *Journal of Materials Science* 28: 2187-2190.

Theiss, F., Apelt, D., Brand, B., Kutter, A., Zlinszky, K., Bohner, M., Matter, S., Frei, C., Auer, J. A. & von Rechenberg, B. 2005. Biocompatibility and resorption of a brushite calcium phosphate cement. *Biomaterials* 26: 4383-4394.

Vallet-Regi, M. & Gonzalez-Calbet, J.M. 2004. Calcium phosphates as substitution of bone tissues. *Progress in Solid State Chemistry* 32: 1-31.

Walsh, D., Kingston, J.L., Heywood, B.R. & Mann, S. 1993. Influence of monosaccharides and related molecules on the morphology of hydroxyapatite. *Journal of Crystal Growth* 133: 1-12.

Wang, Y.J., Lai, C., Wei, K. & Tang, S.Q. 2005. Influence of temperature, ripening time, and cosurfactant on solvothermal synthesis of calcium phosphate nanobelts. *Materials Letters* 59: 1098-1104.

Wang, Y., Zhang, S., Wei, K., Zhao, N., Chen, J. & X. Wang. 2006. Hydrothermal synthesis of hydroxyapatite nanopowders using cationic surfactant as a template. *Materials Letters* 60: 1484-1487.

Weiner, S., Wagner, H.D. 1998. The material bone: structure-mechanical function relations, *Annual Review of Materials Science* 28: 271-298.

Xu, H.H.K. & Simon Jr, C.G. 2005. Fast setting calcium phosphate-chitosan scaffold: mechanical properties and biocompatibility *Biomaterials* 26: 1337-1348.

Zhao, F., Yin, Y., Lu, W.W., Leong, J.C., Zhang, W., Zhang, J., Zhang, M. & Yao K. 2002. Preparation and histological evaluation of biomimetic three-dimensional hydroxyapatite/ chitosan gelatin network composite scaffolds. *Biomaterials* 23: 3227-3234.

H.N. Lim* & A. Kassim
Chemistry Department
Faculty of Science
Universiti Putra Malaysia
43400 UPM Serdang, Selangor Darul Ehsan
Malaysia

N.M. Huang
Solid State Physics Research Laboratory
Physics Department, Faculty of Science
University of Malaya, 50603 Kuala Lumpur
Malaysia

*Corresponding author; email: janet_limhn@yahoo.com

Received: 7 October 2008
Accepted: 14 August 2009